
Zero-to-Hero: Enhancing Zero-Shot Novel View Synthesis via Attention Map Filtering

Ido Sobol¹ Chenfeng Xu² Or Litany^{1,3}

<https://zero2hero-nvs.github.io/>

¹Technion
²UC Berkeley
³NVIDIA

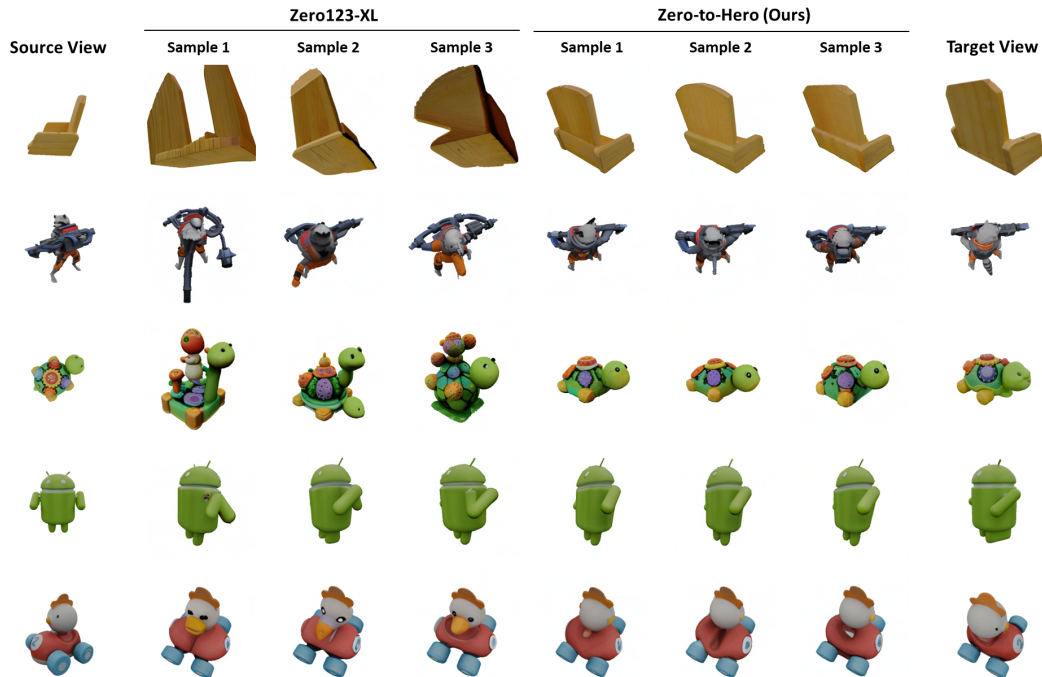


Figure 1: Novel views generated from a single source image (far left column) at a specific target view angle (with different seeds), compared between Zero123-XL [26] and our Zero-to-Hero method. Operating during inference, our method achieves significantly higher fidelity and maintains authenticity to the original image, all while ensuring realistic variation in the results (e.g. variations in chair backs in the top row). The ground-truth target view is displayed in the far right column.

Abstract

Generating realistic images from arbitrary views based on a single source image remains a significant challenge in computer vision, with broad applications ranging from e-commerce to immersive virtual experiences. Recent advancements in diffusion models, particularly the Zero-1-to-3 model, have been widely adopted for generating plausible views, videos, and 3D models. However, these models still

struggle with inconsistencies and implausibility in new views generation, especially for challenging changes in viewpoint. In this work, we propose Zero-to-Hero, a novel test-time approach that enhances view synthesis by manipulating attention maps during the denoising process of Zero-1-to-3. By drawing an analogy between the denoising process and stochastic gradient descent (SGD), we implement a filtering mechanism that aggregates attention maps, enhancing generation reliability and authenticity. This process improves geometric consistency without requiring retraining or significant computational resources. Additionally, we modify the self-attention mechanism to integrate information from the source view, reducing shape distortions. These processes are further supported by a specialized sampling schedule. Experimental results demonstrate substantial improvements in fidelity and consistency, validated on a diverse set of out-of-distribution objects.

1 Introduction

The pursuit of realistic image synthesis at arbitrary views, given only a single source image, has long been a cornerstone challenge in computer vision and graphics. This technology can cater to countless applications, such as interactive product inspection, robot-scene interaction, and immersive virtual experiences. In this work, we aim to advance this important line of research by improving the generation of novel views that are plausible and faithful to the input image. A recent, promising approach, Zero-1-to-3 [26] has developed a foundation model to synthesize novel views based on a single source image and a target view angle. By leveraging a pre-trained, image-conditioned stable diffusion model backbone [3], fine-tuned with target camera poses, and trained on paired source and target views from a vast collection of 3D models [10, 9], Zero-1-to-3 can generalize beyond its training set and generate plausible novel views. As a result, this model has quickly gained popularity, inspiring subsequent work in 3D and 4D scene generation [8, 23, 38, 27, 25, 24, 51, 32, 43, 34, 20].

Despite its remarkable ability, Zero-1-to-3 has been observed to generate views that are implausible, or inconsistent with the input object in terms of shape and appearance [23, 8]. Previous works have tried to mitigate these issues by retraining diffusion models with more data [9] or to generate multiple views [38, 24, 25, 23, 8, 27]. Despite substantial improvement, both approaches are resource-intensive due to the required re-training on large-scale 3D datasets. Another line of work attempts to consolidate inconsistencies across multiple generated views through a 3D representation like NeRF [14, 29]. However, direct aggregation often results in blurry outputs, as observed by [23]. Instead, ViVid-1-to-3 [23] employed a multiview representation that naturally supports the use of a video foundation model. Nevertheless, this approach requires generating the entire trajectory from the source to the target view, adding significant complexity and computational overhead. Notably, the denoising process in Zero-1-to-3 remains unchanged.

In this work, we propose Zero-to-Hero, a novel test-time technique that addresses view synthesis artifacts through attention map manipulation. Recognizing attention maps as crucial for latent predictions, we hypothesize that enhancing robustness in attention maps predictions can significantly reduce generation misalignment. To achieve this, we draw an analogy between the denoising process in diffusion models and stochastic gradient descent (SGD) optimization of neural networks. Specifically, we relate network weights that predict local gradients at each optimization step, based on sampled training examples and labels, to the denoising network’s attention maps that predict latent representations from sampled noise at each denoising step. Inspired by gradient aggregation and weight-averaging techniques that improve prediction robustness (e.g., consistency training [45]), we propose a filtering mechanism to enhance attention map reliability. This mechanism comprises iterative map aggregation within denoising steps and map averaging across denoising steps. The result is more reliable maps, particularly during the early denoising stages when coarse output shapes are determined, leading to more plausible and realistic views.

To further promote consistency with the input, we modify the self-attention operation by running a parallel generation branch using the identity pose, incorporating its keys and values into the attention layer of the target view. Unlike previous applications of this technique [28, 5, 1]), we find it beneficial in view synthesis to limit its use to the early denoising stages, preventing shape distortions. Our unique denoising procedure is further complemented by a novel sampling schedule that emphasizes early and late denoising stages, maximizing performance. Our main contributions are as follows:

- To address the main limitations of the Zero-1-to-3 model, we perform an in-depth analysis and identify self-attention maps as the main candidate for correcting generation artifacts.
- We establish a conceptual analogy between model weights in stochastic gradient descent-based network training and the role of attentions map updates during generation of a denoising diffusion model. Based on this, we propose a simple yet powerful attention map filtering process resulting in enhanced target shape generation. We supplement our filtering technique with identity view information injection and a specialized sampling schedule.
- Our method requires no additional training, and it avoids the overhead of external models or generating multiple views.

Through comprehensive experiments on out-of-distribution objects, we demonstrate that our technique robustifies Zero-1-to-3 and its extended version, Zero123-XL, leading to views that are more faithful to both the input image and desired camera transformation. Our results show significant and consistent improvements across both appearance and shape evaluation metrics.

2 Related Work

2.1 Novel View Synthesis with Diffusion Models

Diffusion models have dominated various generative applications [17, 11, 37, 35, 39]. Particularly, novel-view synthesis, as a core of applications like augmented reality and simulations, naturally enjoys the benefits of high-fidelity zero-shot synthesis with diffusion models. One line of works [48, 26, 42, 22, 49, 23] is to generate a novel-view image given a source image (*i.e.*, image-to-image). These approaches typically involve training a diffusion model conditioned on both an arbitrary camera pose and the source view. For instance, the representative work, Zero-1-to-3, fine-tunes a pre-trained Stable Diffusion model [35] by replacing the text prompt with camera pose and CLIP features[33]. Moreover, another research trajectory [31, 21, 14, 7, 44] proposes generating a 3D representation from a single image (*i.e.*, image-to-3D), which allows for sampling desired views from these 3D models. Our method, Zero-to-Hero, builds on the first approach (specifically Zero-1-to-3 and Zero123-XL) and distinguishes itself by eliminating the need for extensive training. Instead, it offers a test-time, plug-and-play approach that significantly enhances visual quality and consistency.

2.2 Test-Time Refinement in Diffusion-Based Generation

A common test-time refinement strategy in diffusion generation is leveraging guidance [28, 2, 18] to direct the sampling process with additional conditions. For example, Repaint [28] utilizes a mask-then-renoise strategy to refine the generation results. Repaint also introduces a per-step resampling technique, where given a horizon-size h , a latent z_t is re-noised to z_{t+h} and then denoised again to z_t multiple times. They observe that resampling helps to generate more harmonized outputs, given an external guidance or condition. Restart [50] offers a sampling algorithm based on a variation of resampling within a chosen interval of steps. Our method is inspired by the strategy of per-step resampling. We show that it serves as a powerful correction mechanism throughout the generation process, even when no external guidance or condition is provided.

2.3 Attention Map Manipulation in Diffusion Models

Stable Diffusion [35] utilizes attention to enforce the condition information onto the generated results. Previous works demonstrate that manipulating the attention operation can achieve new capabilities [46, 5, 1, 51]. For example, MasaCtrl [5] uses Mutual Self-Attention where source and target images are generated jointly while sharing information, by injecting source image keys and values to the target through self-attention. Here we employ Mutual Self-Attention in the context of novel view synthesis. Differently to prior works we find it beneficial to limit its use to the early denoising stages.

3 Background

3.1 Zero-1-to-3: Challenges and Limitations

Zero-1-to-3 is a pioneering method for novel view synthesis based on a diffusion model, which has gained significant popularity. This model is built upon the image-conditioned variant of Stable

Diffusion (SD) [35], fine-tuned specifically for novel view synthesis. Zero-1-to-3 is conditioned on a source image and relative transformation to the desired view angle $[\mathcal{R}|\mathcal{T}]$. Maintaining the SD architecture, these conditions are integrated in two ways. First, a CLIP [33] embedding of the input image is concatenated with the relative transformation $[\mathcal{R}|\mathcal{T}]$ and mapped to the original CLIP dimension to form a global pose-CLIP embedding, interacting with the UNet layers through cross-attention, enriching the generation with high-level semantic information. In parallel, the input image is channel-concatenated with the denoised image, helping the model preserve the identity and details of the synthesized object.

While Zero-1-to-3 [26] has achieved substantial progress in novel view synthesis, several common issues limit its practical application. Firstly, the generated images might not fit real-world distributions, resulting in implausible and unrealistic outputs (e.g., first row in Fig.1). Secondly, the target image may appear plausible but be inconsistent with the input image in terms of shape or appearance (e.g., fifth row in Fig.1).

In this work, we identify the critical role of self-attention maps in high-quality generation and propose a novel filtering process that enhances robustness without requiring further training. This process addresses the aforementioned issues, ensuring reliable and consistent results.

3.2 Leveraging Gradient and Weight Aggregation for Improved Prediction Consistency

In this work, we draw a conceptual analogy between gradients and weights in stochastic gradient descent (SGD), and latents and attention maps in denoising diffusion models. Leveraging this analogy, we adapt techniques from SGD to enhance prediction consistency in diffusion models. Below, we summarize general techniques in SGD that improve the training process.

SGD is a fundamental tool in network training [4], designed to navigate the weight (network parameter) space towards local minima. For a neural network $F(x; \theta)$ with parameters θ , SGD samples training data points x_i and their corresponding labels y_i , and computes the gradient of the loss function $L(F(x_i; \theta), y_i)$ with respect to θ to update the parameters.

In practice, aggregation of *gradients* and network *weights* during training is often performed to reduce variance and improve convergence. Gradient aggregation typically involves averaging gradient values over a batch, while weight aggregation accounts for the history of the weights in each update.

Notable examples include Stochastic Weight Averaging (SWA) [19] and teacher networks [45] used in consistency training by employing an exponential moving average (EMA) of a student network to maintain high-quality predictions. This technique is prevalent in semi-supervised and representation learning [13, 15, 6]. For a detailed study of EMA in network training, we refer readers to [30].

4 Method

In this work we are concerned with the task of single image novel view synthesis. Formally, given an input image of an object and a relative camera transformation towards a desired target view, our goal is to generate the image at that target view. Specifically, we build upon the seminal work of Zero-1-to-3 [26] which tackled this task via a diffusion model. As detailed in Sec. 3.1 Zero-1-to-3 often struggles to generate plausible and input-consistent images. In this work we propose Zero-to-Hero—a novel training-free technique that significantly improves its generation quality through attention map manipulation. This section is structured as follows. (4.1) through network architecture analysis we identify self-attention maps as key for robust view generation; (4.2) drawing inspiration from SGD convergence-enhancement techniques, we outline our novel attention map filtering pipeline; (4.3) details each step of the map filtering; (4.4) introduces the mutual self-attention which we use for shape guidance at early generation stages; (4.5) Finally, our proposed hourglass scheduler is introduced for more efficient utilization of generation steps. Fig. 2 depicts Zero-to-Hero’s main modules. An ablation of these modules is provided in Tab. 2 and in Sec. A.4 of the appendix.

4.1 Analyzing the Role of Cross- and Self-Attention Layers in Novel View Generation

Zero-1-to-3 builds upon the image-to-image variant of Stable Diffusion [35], which utilizes a UNet [36] architecture as its backbone and incorporates both self- and cross-attention layers. In this subsection, we analyze the roles of these components and their contributions to the generated view. This analysis aims to identify effective intervention points for enhancing generation quality.

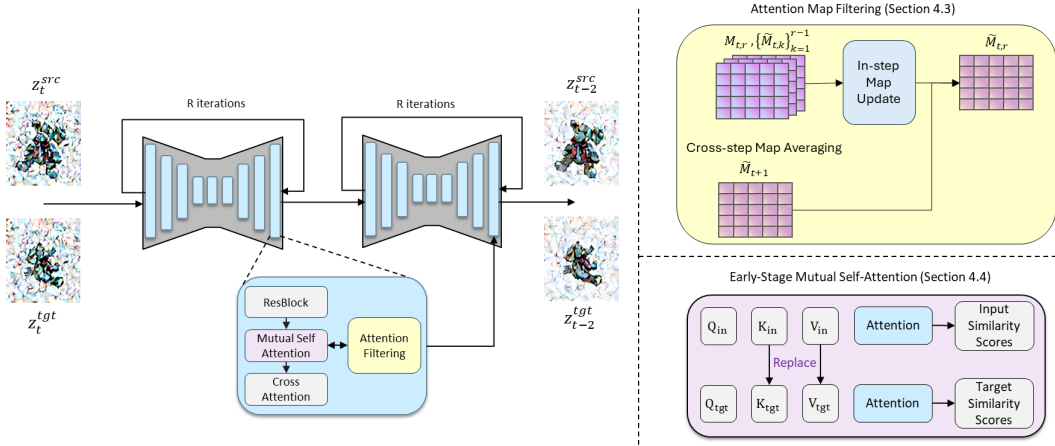


Figure 2: **Zero-to-Hero main modules.** (Left) Two denoising steps of the generation process of both the source (top) and target views (bottom). Each denoising step is iterated R times (“resampling”). (Right-top) **Attention map filtering:** Robustifying attention maps via an aggregation of same step and previous steps attention maps. (Right-bottom) **Mutual self-attention:** Guiding target shape through the keys and values of the source generation branch.

Global pose conditioning through cross-attention. Prior work [16] has demonstrated that the cross-attention layers in text-to-image diffusion models, which link text tokens to the latent image, are spatially aware and can be used for spatial manipulation. We first investigate these cross-attention layers, as they are the only components in the model through which the target pose is injected. In the text-to-image variant of Stable Diffusion, the generation is conditioned on a prompt \mathcal{P} containing C tokens, each encoded with CLIP into an embedding, resulting in a condition $c_{T2I} \in \mathbb{R}^{C \times d_{CLIP}}$. However, in Zero-1-to-3, the condition is a pose-CLIP embedding $c \in \mathbb{R}^{1 \times d_{CLIP}}$, project to keys $K_t \in \mathbb{R}^{1 \times d}$. Formally, given a sample $z_t \in \mathbb{R}^{H \times W \times d_z}$ and its corresponding queries $Q_t \in \mathbb{R}^{H \times W \times d}$, the pre-softmax attention map \mathcal{A} between Q_t and K_t has dimensions $H \times W \times 1$. Given that the summation of the softmax is always 1, the post-softmax attention map $\text{softmax}(\mathcal{A})$ in Zero-1-to-3 is a constant all-ones matrix. A visual demonstration is presented in Fig. 6 in the appendix.

The post-softmax attention map is used to compute a weighted sum over the values matrix $V \in \mathbb{R}^{1 \times d}$, obtained by a transformation of the condition c . Since the attention matrix is an all-ones matrix, we conclude that the cross-attention operation degenerates into a global bias term, lacking spatially aware operations. Computing similarity scores in the cross-attention layers is redundant as these scores are never used. While in principle it is possible to improve the global bias term by additional optimization objectives and extra training overhead, we focus on the self-attention layers to enhance the results and mitigate the consistency issues while avoiding retraining the model.

Spatial information flow through self-attention. By monitoring the self-attention layers during the generation process, we observe that random noise introduced to the latent representation also introduces randomness to the attention maps. This randomness, while promoting generation diversity, can often lead to undesired strong correlations, that are misaligned with the true target. These strong correlations may persist through the denoising process, resulting in accumulated errors and visual artifacts.

Given the above observation and the insight about the spatial-degeneracy in the cross-attention layers, we hypothesize that the self-attention layers preserve the information about the structure and geometry of the generated image, through the similarity scores between different elements in the latent vector. To validate our hypothesis, we conduct a straightforward experiment to assess Zero-1-to-3’s performance using the ‘ground truth’ self-attention maps, which reflect the most accurate connections considering the true target image. Specifically, we selected two images, I^{src} and I^{tgt} , with known relative camera parameters $[\mathcal{R}|\mathcal{T}]$. We first encode I^{tgt} to obtain the clean latent z_0^{tgt} and then add subtle noise to obtain the corresponding noisy latent for timestep τ_{init} , z_{init}^{tgt} . A single denoising step is performed on the noisy latent, and we save the self-attention maps from each layer in the UNet,



Figure 3: Through the injection of ground-truth attention maps extracted from the target view, we demonstrate that **Self-attention maps are key to robust view synthesis**.

considering these maps as the ground truth (GT) maps. In our experiments, $\tau_{\text{init}} = 5$. Next, we sample random Gaussian noise and denoise it to regenerate the target image. During each denoising step, we replace the computed self-attention maps with the GT maps, without altering any other components (e.g., cross-attention layers, residual blocks) or the latents, queries, keys, and values. We report the results in the experiment section in Tab. 1, showing a significant improvement in all metrics. Note that the results obtained with the GT attention maps are a strict upper bound, as the GT maps contain information about areas that are invisible in the source view. Our experiment validates that through improved self-attention maps, the generated image becomes more plausible. Visual examples are shown in Fig. 3 and in Fig. 7 in the appendix, refer to Fig. 1 for the results of Zero123-XL and Zero-to-Hero for the same views.

4.2 From SGD to Diffusion Models: Attention Map Filtering as Weight-Space Manipulation

We draw a conceptual analogy between a denoising process of a diffusion model, and SGD based network optimization as both progress through gradient prediction of a loss function, and log probability (the score)[41], respectively. Building on the discussion from the previous section, we treat the self-attention maps as parameters M in the denoising process $z_{t-1} = \mu(z_t; M_t, \psi)$ and define their update process as a mapping¹: $M_t \rightarrow z_{t-1} \rightarrow M_{t-1}$. Here the map M_{t-1} results from passing the latent z_{t-1} through the attention layers. This process is analogous to gradient descent optimization in neural networks, where each step adjusts the weights in the direction of the gradient of a loss function, such as the log probability in classification tasks. We denote this weight update as a mapping $\theta_t \rightarrow \hat{y}_t \rightarrow \theta_{t+1}$, where $\hat{y}_t = F(x_t; \theta)$, and the updated parameters θ_{t+1} result from a gradient step.

As detailed in Sec. 3.2, gradient and weight aggregation are essential for robust convergence. We outline this process in three steps illustrating the analogy between network parameter updates and attention map filtering. Fig. 4 further illustrates the analogy.

Step-by-Step Analogy From network parameters to attention maps

Network Training

- 1: **Sampling**: Generate R pairs of samples and their corresponding labels $\{(x_i, y_i)\}_{i=1}^R$.
- 2: **In-step weight update**: Average the gradients to adjust the network parameters: $\tilde{\theta}_t = \theta_t - \lambda \sum \nabla_{\theta} L(F(x_i; \theta_t), y_i)$.
- 3: **Cross-step weight averaging**: Update network parameters using EMA: $\theta_{t+1} = \alpha \theta_t + (1 - \alpha) \tilde{\theta}_t$, for $\alpha \in [0, 1]$.

Denoising Process

- 1: **(Re-)Sampling**: Repeatedly re-noise z_{t-1} to z_t and denoise, R times.
 - 2: **In-step map update**: Resampling results in a sequence of maps $\{M_{t,r}\}_{r=1}^R$, aggregated into the final updated prediction $\tilde{M}_{t,R}$.
 - 3: **Cross-step map averaging**: Update attention maps via EMA: $\tilde{M}_{t-1} = \alpha M_t + (1 - \alpha) \tilde{M}_{t-1}$, for $\alpha \in [0, 1]$.
-

4.3 Robust View Generation via Attention Map Filtering

We now discuss in detail each of the map filtering steps. A scheme of the different filtering modules is provided in Fig. 2(Left, and Top-right).

Latent refinement via per-step resampling. Inspired by previous studies [28, 2], we implement per-step resampling throughout the image generation process. We select a range of timesteps

¹Although the latent prediction z_{t-1} depends on the parameters ψ of denoising UNet μ , they remain unchanged. Here we emphasize that the attention maps M are the parameters being updated.

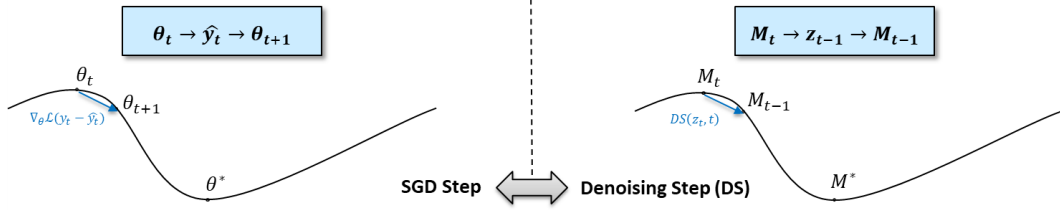


Figure 4: From SGD to Diffusion Models: An illustration of our conceptual analogy.

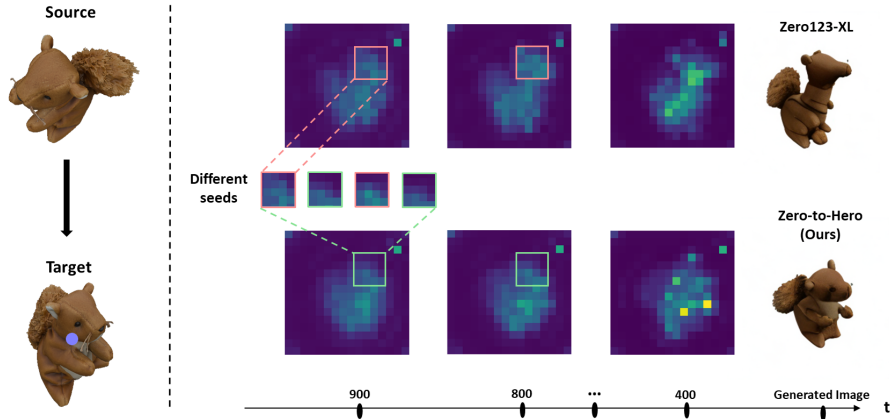


Figure 5: **Attention map filtering in action.** We compare the attention scores of zero123-XL (top) and Zero-to-Hero (bottom) wrt the region marked with a purple circle at different denoising steps. Both methods are initialized with the same seed. We observe that the strong correlation values in the upper right corner lead to exaggerated content creation (note the unrealistically elongated neck). Conversely, through filtering, Zero-to-Hero mitigates these artifacts, leading to robust view synthesis.

$[t_{min}, t_{max}]$, where each denoised sample z_t is re-noised with the proper noise ratio to the previous sampled timestep z_{t+1} and denoised back to z_t for R iterations². We concur with previous studies that resampling functions as an effective corrective mechanism to the generated image, as can be seen in Tab. 2). Experimentally, we find that it is particularly useful during the *initial stages* of the denoising process. Through resampling we progressively generate R attention maps with different noise patterns. We propose to leverage these intermediate maps to further boost performance through in- and cross-step attention map manipulations.

In-step map update. We propose a novel attention pooling function f , to update the attention maps within the denoising step. Specifically, a self-attention map is refined based on previous maps $\{M_{t,k}\}_{k=1}^{r-1}$ created at the same timestep. Since resampling is a sequential process, we perform a progressive aggregation scheme: $\widetilde{M}_{t,r} = f(M_{t,r}, \{\widetilde{M}_{t,k}\}_{k=1}^{r-1})$. We found the element-wise min-pooling operator $f(a, b) = \min(a, b)$ to perform best in our experiments. We discuss other options for f in the appendix.

Cross-step map averaging. Resampling tends to favour “conservative” generations, often gradually neglecting fine image details like buttons and eyes as denoising progresses. This phenomenon it not resolved by the in-step update. To mitigate this issue, we propose to pass the self-attention map at time t , \widetilde{M}_t to the next step in the denoising process. We implement this cross-step aggregation via EMA: $\widetilde{M}_{t-1} = \alpha M_t + (1 - \alpha) \widetilde{M}_{t-1}$, for $\alpha \in [0, 1]$. This method effectively balances past priors with current data to enhance the denoising results. In practice we apply both methods in tandem, as detailed in Sec. A.3. An example of our attention filtering is presented in Fig. 5.

²Depending on the sampling algorithm, $h \geq 1$ steps may be taken.

4.4 Early-Stage Shape Guidance via Mutual Self-Attention

Of the two challenges describe in the introduction, attention map filtering handles well generating realistic outputs. Yet, we observe it is insufficient to enforce consistency with the input shape and appearance. To that end, we propose to utilize mutual self-attention to propagate information from the input to the generated view. Similar to prior works [46, 5, 1, 51], we generate the input and target views in parallel. At each timestep t , we obtain queries, keys and values of the self-attention layers for both the input and the target branches. Similar to the mutual self-attention introduced in [5], we modify the self-attention operation of the target: $Attn(Q^{tgt}, K^{in}, V^{in})$ (See Fig. 2(bottom-right)).

Previous studies initiate mutual self-attention at a later denoising step after the structure of the target has been formed. Conversely, in our case, to guide the structure of the target to be more consistent with the input, we find it more effective when applied from the beginning of the denoising process, and rather terminate it once the structure has been stabilized.

4.5 Hourglass Sampling Scheduler

As resampling is a time-consuming operation, significantly increasing the number of function evaluation (NFE), we seek an efficient scheduling scheme that will enable robust and high quality generation, while preserving the fast generation times of Zero-1-to-3. We use the common DDIM sampling [40], and propose an efficient scheduling scheme to select the sampled timesteps. In the experiments section, we demonstrate that increasing the number of denoising steps does not necessarily improve the performance, and therefore we aim to use an overall small number of sampled timesteps. Specifically, we find that denser sampling during the beginning of the denoising process is crucial to promote realism. We also find that denser sampling at the final steps enhances fine details. Therefore, we suggest a double heavy-tailed scheduling scheme we call *Hourglass*, according to which we divide the generation process into 3 stages, as detailed in A.3. Within each stage, we sample steps uniformly via DDIM. However, in the first and last stages we sample steps more densely (at a higher rate) than in the middle stage, by a factor of λ_{den} .

5 Experiments

Dataset. We evaluate our method using the Google Scanned Objects (GSO) Dataset [12], which includes 1030 scanned household objects, following previous works. However, the dataset’s imbalance (e.g., 254 objects are categorized as “shoe”) and the high proportion of symmetrical shapes limit its reliability for evaluation. To address this, inspired by [23], we select a challenging subset of 50 objects from GSO, avoiding symmetrical and repetitive shapes. For each object, we render 8 random views (details in Sec. A.6 of the appendix) and synthesize the remaining views from each source view, generating each target view with 3 different seeds to calculate the average score per measure.

Metrics. We report the standard image quality metrics PSNR, SSIM [47] and LPIPS [52]. As these metrics are sensitive to slight color variations, we segment the generated targets and their corresponding real images, via thresholding, and report the Intersection Over Union (IoU) score.

5.1 Evaluations

Quantitative evaluation. We evaluate Zero-to-Hero against zero-1-to-3 and on zero123-XL. In Tab. 1 we report all metrics for the original models using 25, 50 and 100 DDIM steps, and for our method applied to both models. We include the number of sampled timesteps T and the total number of network evaluation NFE (accounting for resampling). Zero-to-Hero consistently improves performance across all metrics, taking a significant step towards bridging the performance gap to GT attention maps. All implementation details are provided in Sec. A.3 of the appendix.

Qualitative evaluation. In Fig. 1, we visually demonstrate how Zero-to-Hero is able to mitigate various artifacts generated by Zero-1-to-3, from implausible results to incorrect poses. We present 3 examples per target view, generated with 3 random seeds, to emphasize the consistency and robustness our method offers.

5.2 Ablation Study

To assess the contribution of Zero-to-Hero different components to the final performance, we evaluate our pipeline on a subset of 10 challenging objects from our data, starting from the baseline Zero123-

Table 1: **Quantitative evaluation on a challenging GSO subset.** Zero-to-Hero consistently improves performance upon baselines, taking a significant step towards oracle map performance (bottom rows).

Name	T	NFE	PSNR \uparrow	SSIM \uparrow	LPIPS \downarrow	IOU \uparrow
Zero-1-to-3	25	25	17.27	0.851	0.173	73.5%
Zero-1-to-3	50	50	17.24	0.850	0.173	73.5%
Zero-1-to-3	100	100	17.21	0.850	0.173	73.4%
Ours (Zero-1-to-3)	26	66	17.64	0.859	0.163	75.2%
Zero123-XL	25	25	17.72	0.854	0.163	76.4%
Zero123-XL	50	50	17.71	0.854	0.162	76.4%
Zero123-XL	100	100	17.68	0.854	0.163	76.4%
Ours (Zero123-XL)	26	66	18.35	0.864	0.153	78.3%
Zero-1-to-3 + GT maps	50	50	21.52	0.888	0.122	88.8%
Zero123-XL + GT maps	50	50	21.79	0.890	0.117	88.6%

XL and gradually adding each module. The results are summarized in Tab. 2. When reporting the results of the vanilla Zero123-XL, we use its *best* score achieved by running the model with 25, 50, and 100 steps. A similar comparison against zero-1-to-3 is included in Sec. A.4 of the appendix, demonstrating consistent behavior. We also analyze the affect of resampling and our attention filtering on the *generation diversity* in Sec. A.5 of the appendix.

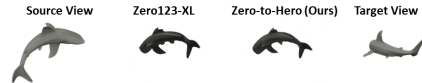
Table 2: **Ablation Study.** We demonstrate the importance of each of Zero-to-Hero modules, applied to the base method Zero123-XL: Sample scheduling (Hourglass), Resampling (Resample), Attention map filtering (AMF), and Early stage Mutual Self-Attention (MSA). Consistent conclusions are reached with the base model Zero-1-to-3 and are shown in Sec. A.4 of the appendix.

Hourglass	Resample	AMF	MSA	PSNR \uparrow	SSIM \uparrow	LPIPS \downarrow	IOU \uparrow
×	×	×	×	17.16	0.856	0.173	77.8%
✓	×	×	×	17.18	0.857	0.172	78.0%
✓	✓	×	×	17.44	0.859	0.169	78.6%
✓	✓	✓	×	17.58	0.861	0.165	79.6%
✓	✓	×	✓	17.82	0.866	0.161	79.7%
✓	✓	✓	✓	17.90	0.867	0.159	80.3%

6 Conclusions and Future Work

In this paper, we introduced Zero-to-Hero, a training-free method to boost the robustness of novel view synthesis. We enhanced the performance of a pre-trained Zero-1-to-3 diffusion model using two key innovations: a test-time attention map filtering mechanism that enhances output realism, and an effective use of source view information to improve input consistency. Our approach also features a novel timestep scheduler for maintaining computational efficiency. In future work, we aim to refine our method by developing trainable filtering mechanisms, enhancing pose authenticity via cross-attention manipulation, and extending our approach to other diffusion-based generative tasks.

Limitations. Our method, operating at test-time, is limited by the generative capabilities of the pre-trained model. If Zero-1-to-3 cannot correctly generate the target pose, our method may not enhance the output, as demonstrated in the inset figure.



7 Acknowledgments

We sincerely thank Matan Atzmon for impactful discussions and James Lucas for his invaluable feedback. Or Litany is a Taub fellow and is supported by the Azrieli Foundation Early Career Faculty Fellowship.

References

- [1] Yuval Alaluf, Daniel Garibi, Or Patashnik, Hadar Averbuch-Elor, and Daniel Cohen-Or. Cross-image attention for zero-shot appearance transfer. arXiv preprint arXiv:2311.03335, 2023.
- [2] Arpit Bansal, Hong-Min Chu, Avi Schwarzschild, Soumyadip Sengupta, Micah Goldblum, Jonas Geiping, and Tom Goldstein. Universal guidance for diffusion models. In Proceedings of the IEEE/CVF Conference on Computer Vision and Pattern Recognition, pages 843–852, 2023.
- [3] Andreas Blattmann, Tim Dockhorn, Sumith Kulal, Daniel Mendelevitch, Maciej Kilian, Dominik Lorenz, Yam Levi, Zion English, Vikram Voleti, Adam Letts, et al. Stable video diffusion: Scaling latent video diffusion models to large datasets. arXiv preprint arXiv:2311.15127, 2023.
- [4] Léon Bottou. Large-scale machine learning with stochastic gradient descent. In Proceedings of COMPSTAT’2010: 19th International Conference on Computational Statistics Paris France, August 22-27, 2010 Keynote, Invited and Contributed Papers, pages 177–186. Springer, 2010.
- [5] Mingdeng Cao, Xintao Wang, Zhongang Qi, Ying Shan, Xiaohu Qie, and Yinqiang Zheng. Masactrl: Tuning-free mutual self-attention control for consistent image synthesis and editing. In Proceedings of the IEEE/CVF International Conference on Computer Vision, pages 22560–22570, 2023.
- [6] Mathilde Caron, Hugo Touvron, Ishan Misra, Hervé Jégou, Julien Mairal, Piotr Bojanowski, and Armand Joulin. Emerging properties in self-supervised vision transformers. In Proceedings of the IEEE/CVF international conference on computer vision, pages 9650–9660, 2021.
- [7] Eric R Chan, Koki Nagano, Matthew A Chan, Alexander W Bergman, Jeong Joon Park, Axel Levy, Miika Aittala, Shalini De Mello, Tero Karras, and Gordon Wetzstein. Generative novel view synthesis with 3d-aware diffusion models. In Proceedings of the IEEE/CVF International Conference on Computer Vision, pages 4217–4229, 2023.
- [8] Yabo Chen, Jiemin Fang, Yuyang Huang, Taoran Yi, Xiaopeng Zhang, Lingxi Xie, Xinggang Wang, Wenrui Dai, Hongkai Xiong, and Qi Tian. Cascade-zero123: One image to highly consistent 3d with self-prompted nearby views. arXiv preprint arXiv:2312.04424, 2023.
- [9] Matt Deitke, Ruoshi Liu, Matthew Wallingford, Huong Ngo, Oscar Michel, Aditya Kusupati, Alan Fan, Christian Laforte, Vikram Voleti, Samir Yitzhak Gadre, et al. Objaverse-xl: A universe of 10m+ 3d objects. Advances in Neural Information Processing Systems, 36, 2024.
- [10] Matt Deitke, Dustin Schwenk, Jordi Salvador, Luca Weihs, Oscar Michel, Eli VanderBilt, Ludwig Schmidt, Kiana Ehsani, Aniruddha Kembhavi, and Ali Farhadi. Objaverse: A universe of annotated 3d objects. In Proceedings of the IEEE/CVF Conference on Computer Vision and Pattern Recognition, pages 13142–13153, 2023.
- [11] Prafulla Dhariwal and Alexander Nichol. Diffusion models beat gans on image synthesis. Advances in neural information processing systems, 34:8780–8794, 2021.
- [12] Laura Downs, Anthony Francis, Nate Koenig, Brandon Kinman, Ryan Hickman, Krista Reymann, Thomas B McHugh, and Vincent Vanhoucke. Google scanned objects: A high-quality dataset of 3d scanned household items. In 2022 International Conference on Robotics and Automation (ICRA), pages 2553–2560. IEEE, 2022.
- [13] Jean-Bastien Grill, Florian Strub, Florent Altché, Corentin Tallec, Pierre Richemond, Elena Buchatskaya, Carl Doersch, Bernardo Avila Pires, Zhaohan Guo, Mohammad Gheshlaghi Azar, et al. Bootstrap your own latent—a new approach to self-supervised learning. Advances in neural information processing systems, 33:21271–21284, 2020.
- [14] Jiatao Gu, Alex Trevithick, Kai-En Lin, Joshua M Susskind, Christian Theobalt, Lingjie Liu, and Ravi Ramamoorthi. Nerfdiff: Single-image view synthesis with nerf-guided distillation from 3d-aware diffusion. In International Conference on Machine Learning, pages 11808–11826. PMLR, 2023.

- [15] Kaiming He, Haoqi Fan, Yuxin Wu, Saining Xie, and Ross Girshick. Momentum contrast for unsupervised visual representation learning. In Proceedings of the IEEE/CVF conference on computer vision and pattern recognition, pages 9729–9738, 2020.
- [16] Amir Hertz, Ron Mokady, Jay Tenenbaum, Kfir Aberman, Yael Pritch, and Daniel Cohen-Or. Prompt-to-prompt image editing with cross attention control. arXiv preprint arXiv:2208.01626, 2022.
- [17] Jonathan Ho, Ajay Jain, and Pieter Abbeel. Denoising diffusion probabilistic models. Advances in neural information processing systems, 33:6840–6851, 2020.
- [18] Jonathan Ho and Tim Salimans. Classifier-free diffusion guidance. arXiv preprint arXiv:2207.12598, 2022.
- [19] Pavel Izmailov, Dmitrii Podoprikin, Timur Garipov, Dmitry Vetrov, and Andrew Gordon Wilson. Averaging weights leads to wider optima and better generalization. arXiv preprint arXiv:1803.05407, 2018.
- [20] Yanqin Jiang, Li Zhang, Jin Gao, Weimin Hu, and Yao Yao. Consistent4d: Consistent 360 $\{\deg\}$ dynamic object generation from monocular video. arXiv preprint arXiv:2311.02848, 2023.
- [21] Heewoo Jun and Alex Nichol. Shap-e: Generating conditional 3d implicit functions. arXiv preprint arXiv:2305.02463, 2023.
- [22] Yash Kant, Aliaksandr Siarohin, Michael Vasilkovsky, Riza Alp Guler, Jian Ren, Sergey Tulyakov, and Igor Gilitschenski. invs: Repurposing diffusion inpainters for novel view synthesis. In SIGGRAPH Asia 2023 Conference Papers, pages 1–12, 2023.
- [23] Jeong-gi Kwak, Erqun Dong, Yuhe Jin, Hanseok Ko, Shweta Mahajan, and Kwang Moo Yi. Vivid-1-to-3: Novel view synthesis with video diffusion models. arXiv preprint arXiv:2312.01305, 2023.
- [24] Minghua Liu, Ruoxi Shi, Linghao Chen, Zhuoyang Zhang, Chao Xu, Xinyue Wei, Hansheng Chen, Chong Zeng, Jiayuan Gu, and Hao Su. One-2-3-45++: Fast single image to 3d objects with consistent multi-view generation and 3d diffusion. arXiv preprint arXiv:2311.07885, 2023.
- [25] Minghua Liu, Chao Xu, Haian Jin, Linghao Chen, Mukund Varma T, Zexiang Xu, and Hao Su. One-2-3-45: Any single image to 3d mesh in 45 seconds without per-shape optimization. Advances in Neural Information Processing Systems, 36, 2024.
- [26] Ruoshi Liu, Rundi Wu, Basile Van Hoorick, Pavel Tokmakov, Sergey Zakharov, and Carl Vondrick. Zero-1-to-3: Zero-shot one image to 3d object. In ICCV, 2023.
- [27] Yuan Liu, Cheng Lin, Zijiao Zeng, Xiaoxiao Long, Lingjie Liu, Taku Komura, and Wenping Wang. Syncdreamer: Generating multiview-consistent images from a single-view image. arXiv preprint arXiv:2309.03453, 2023.
- [28] Andreas Lugmayr, Martin Danelljan, Andres Romero, Fisher Yu, Radu Timofte, and Luc Van Gool. Repaint: Inpainting using denoising diffusion probabilistic models. In Proceedings of the IEEE/CVF conference on computer vision and pattern recognition, pages 11461–11471, 2022.
- [29] Ben Mildenhall, Pratul P Srinivasan, Matthew Tancik, Jonathan T Barron, Ravi Ramamoorthi, and Ren Ng. Nerf: Representing scenes as neural radiance fields for view synthesis. Communications of the ACM, 65(1):99–106, 2021.
- [30] Daniel Morales-Brotons, Thijs Vogels, and Hadrien Hendrikx. Exponential moving average of weights in deep learning: Dynamics and benefits. Transactions on Machine Learning Research, 2024.
- [31] Alex Nichol, Heewoo Jun, Prafulla Dhariwal, Pamela Mishkin, and Mark Chen. Point-e: A system for generating 3d point clouds from complex prompts. arXiv preprint arXiv:2212.08751, 2022.

- [32] Guocheng Qian, Jinjie Mai, Abdullah Hamdi, Jian Ren, Aliaksandr Siarohin, Bing Li, Hsin-Ying Lee, Ivan Skorokhodov, Peter Wonka, Sergey Tulyakov, et al. Magic123: One image to high-quality 3d object generation using both 2d and 3d diffusion priors. arXiv preprint arXiv:2306.17843, 2023.
- [33] Alec Radford, Jong Wook Kim, Chris Hallacy, Aditya Ramesh, Gabriel Goh, Sandhini Agarwal, Girish Sastry, Amanda Askell, Pamela Mishkin, Jack Clark, et al. Learning transferable visual models from natural language supervision. In International conference on machine learning, pages 8748–8763. PMLR, 2021.
- [34] Jiawei Ren, Liang Pan, Jiaxiang Tang, Chi Zhang, Ang Cao, Gang Zeng, and Ziwei Liu. Dreamgaussian4d: Generative 4d gaussian splatting. arXiv preprint arXiv:2312.17142, 2023.
- [35] Robin Rombach, Andreas Blattmann, Dominik Lorenz, Patrick Esser, and Björn Ommer. High-resolution image synthesis with latent diffusion models. In Proceedings of the IEEE/CVF conference on computer vision and pattern recognition, pages 10684–10695, 2022.
- [36] Olaf Ronneberger, Philipp Fischer, and Thomas Brox. U-net: Convolutional networks for biomedical image segmentation. In Medical image computing and computer-assisted intervention—MICCAI 2015: 18th international conference, Munich, Germany, October 5-9, 2015, proceedings, part III 18, pages 234–241. Springer, 2015.
- [37] Chitwan Saharia, William Chan, Saurabh Saxena, Lala Li, Jay Whang, Emily L Denton, Kamyar Ghasemipour, Raphael Gontijo Lopes, Burcu Karagol Ayan, Tim Salimans, et al. Photorealistic text-to-image diffusion models with deep language understanding. Advances in neural information processing systems, 35:36479–36494, 2022.
- [38] Ruoxi Shi, Hansheng Chen, Zhuoyang Zhang, Minghua Liu, Chao Xu, Xinyue Wei, Linghao Chen, Chong Zeng, and Hao Su. Zero123++: a single image to consistent multi-view diffusion base model. arXiv preprint arXiv:2310.15110, 2023.
- [39] Uriel Singer, Adam Polyak, Thomas Hayes, Xi Yin, Jie An, Songyang Zhang, Qiyuan Hu, Harry Yang, Oron Ashual, Oran Gafni, Devi Parikh, Sonal Gupta, and Yaniv Taigman. Make-a-video: Text-to-video generation without text-video data. In The Eleventh International Conference on Learning Representations, 2023.
- [40] Jiaming Song, Chenlin Meng, and Stefano Ermon. Denoising diffusion implicit models. arXiv preprint arXiv:2010.02502, 2020.
- [41] Yang Song and Stefano Ermon. Generative modeling by estimating gradients of the data distribution. Advances in neural information processing systems, 32, 2019.
- [42] Bernard Spiegl, Andrea Perin, Stéphane Deny, and Alexander Ilin. Viewfusion: Learning composable diffusion models for novel view synthesis. arXiv preprint arXiv:2402.02906, 2024.
- [43] Jiaxiang Tang, Jiawei Ren, Hang Zhou, Ziwei Liu, and Gang Zeng. Dreamgaussian: Generative gaussian splatting for efficient 3d content creation. arXiv preprint arXiv:2309.16653, 2023.
- [44] Junshu Tang, Tengfei Wang, Bo Zhang, Ting Zhang, Ran Yi, Lizhuang Ma, and Dong Chen. Make-it-3d: High-fidelity 3d creation from a single image with diffusion prior. In Proceedings of the IEEE/CVF International Conference on Computer Vision, pages 22819–22829, 2023.
- [45] Antti Tarvainen and Harri Valpola. Mean teachers are better role models: Weight-averaged consistency targets improve semi-supervised deep learning results. Advances in neural information processing systems, 30, 2017.
- [46] Narek Tumanyan, Michal Geyer, Shai Bagon, and Tali Dekel. Plug-and-play diffusion features for text-driven image-to-image translation. In Proceedings of the IEEE/CVF Conference on Computer Vision and Pattern Recognition, pages 1921–1930, 2023.
- [47] Zhou Wang, A.C. Bovik, H.R. Sheikh, and E.P. Simoncelli. Image quality assessment: from error visibility to structural similarity. IEEE Transactions on Image Processing, 13(4):600–612, 2004.

- [48] Daniel Watson, William Chan, Ricardo Martin-Brualla, Jonathan Ho, Andrea Tagliasacchi, and Mohammad Norouzi. Novel view synthesis with diffusion models. arXiv preprint arXiv:2210.04628, 2022.
- [49] Chenfeng Xu, Huan Ling, Sanja Fidler, and Or Litany. 3difftection: 3d object detection with geometry-aware diffusion features. CVPR, 2023.
- [50] Yilun Xu, Mingyang Deng, Xiang Cheng, Yonglong Tian, Ziming Liu, and Tommi Jaakkola. Restart sampling for improving generative processes. Advances in Neural Information Processing Systems, 36:76806–76838, 2023.
- [51] Junwu Zhang, Zhenyu Tang, Yatian Pang, Xinhua Cheng, Peng Jin, Yida Wei, Wangbo Yu, Munan Ning, and Li Yuan. Repaint123: Fast and high-quality one image to 3d generation with progressive controllable 2d repainting. arXiv preprint arXiv:2312.13271, 2023.
- [52] Richard Zhang, Phillip Isola, Alexei A Efros, Eli Shechtman, and Oliver Wang. The unreasonable effectiveness of deep features as a perceptual metric. In Proceedings of the IEEE conference on computer vision and pattern recognition, pages 586–595, 2018.

A Appendix

A.1 Cross-Attention in Zero-1-to-3

We demonstrate the degenerated cross-attention layers in Zero-1-to-3 in Fig. 6. We generate a random target view using Zero123-XL and extract the cross-attention map generated at timestep 900 in the last layer of the UNet. The same behaviour holds across all timesteps and layers. The displayed map is created by averaging over all the attention heads.

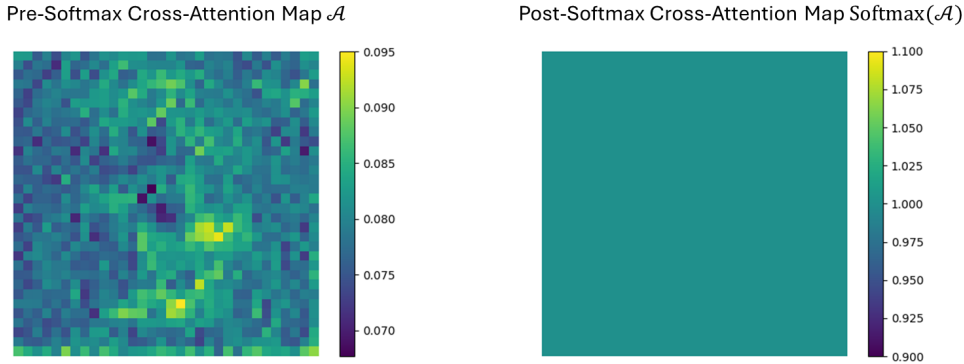


Figure 6: **Cross-Attention in Zero-1-to-3.** (Left) The cross-attention map before applying softmax. (Right) The degenerated all-ones attention map, produced by applying softmax on the left map.

A.2 Self-Attention in Zero-1-to-3

In Fig. 7 we present additional examples showing the performance of Zero123-XL when the self-attention maps are replaced with the 'ground truth' maps, extracted from the real target as described in Sec. 4.1.



Figure 7: Through the injection of ground-truth attention maps extracted from the target view, we demonstrate that **self-attention maps are key to robust view synthesis.**

A.3 Implementation Details

We evaluated our method on the default checkpoint of Zero-1-to-3 and on Zero123-XL. We used the same hyper-parameters for both models, as follows. All experiments were run on a single NVIDIA RTX 4090.

Note that the length of the forward process of Stable Diffusion is $T = 1000$.

Attention map filtering pipeline. As mentioned in the method section of the main paper, we apply both in-step and cross-step aggregation in tandem. In detail, we preserve attention map history

information denoted as H_t . Subsequently, we integrate this historical information through a simple blending technique at each denoising step, along with our in-step map update:

$$\widetilde{M}_{t,r} = \alpha_c \cdot f(M_{t,r}, \{\widetilde{M}_{t,k}\}_{k=1}^{r-1}) + (1 - \alpha_c) \cdot H_{t+1},$$

where $\alpha_c \in [0, 1]$, f is an attention pooling function and $t + 1$ represents the previous sampled step.

The historical information is updated at the last resampling iteration (the R-th iteration) of each timestep as follows: $H_t = \alpha_h \cdot \widetilde{M}_{t,R} + (1 - \alpha_h) \cdot H_{t+1}$, where α_h is a decay factor within the range $[0, 1]$. This historical data is initialized from the first refined self-attention map at the final resampling step, expressed as $H_T = \widetilde{M}_{T,R}$.

Resampling is performed during timesteps $t \in [800, 1000]$, with $R=5$.

In-step map update. In-step map update is applied at timesteps $t \in [800, 1000]$, with element-wise min-pooling as a denoising function in all our experiments. We find that min-pooling is useful during the earlier steps of the denoising, where the noise is substantial.

We explored several simple denoising functions:

1. Averaging: $\widetilde{M}_{t,r} = \frac{1}{r}(M_{t,r} + \sum_{k=1}^{r-1} \widetilde{M}_{t,k})$, which can be extended to weighted averaging.
2. Min pooling: $\widetilde{M}_{t,r} = \min(M_{t,r}, \{\widetilde{M}_{t,k}\}_{k=1}^{r-1})$.
3. Exponential Moving Average: $\widetilde{M}_{t,r} = \alpha_i \cdot M_{t,r} + (1 - \alpha_i) \cdot \widetilde{M}_{t,r-1}$, for $\alpha_i \in [0, 1]$.

While all three improved performance over vanilla resampling, we find min-pooling to work best during the early stages of the denoising process.

Cross-step map averaging. We perform cross-step information passing at timesteps $t \in [600, 1000]$, with $\alpha_h = 0.5$ and $\alpha_c = 0.2$.

Early-stage mutual self-attention. We apply Early-Stage mutual self-attention on timesteps $t \in [600, 1000]$. As mentioned in Sec. 3, the input latent vector is concatenated to the generated latent vector in Zero-1-to-3. Therefore, the target queries contain information about the input view, introducing a bias towards the input view during the generation process. Although mutual self-attention manages to enforce consistency with the input, it sometimes causes pose shifts and visual artifacts. Therefore, We only apply mutual self-attention in the decoder layers of the UNet with spatial resolution of 16×16 and 32×32 (the two largest resolutions, since the latent dimension of Zero-1-to-3 is 32×32).

Hourglass scheduling. We divide the denoising process into 3 generation stages. We define the early stage during timesteps $t \in [\tau_e, \tau_T]$, where the general shape and geometry are determined. τ_T is the length of the forward process [17, 40]. We define the middle stage for $t \in [\tau_m, \tau_e]$, where both the shape and appearance are refined gradually. We define the last stage for $t \in [0, \tau_m]$, where mostly fine-details are refined and added. As describes in the main paper, within each stage we sample steps uniformly via DDIM sampling. However, the sampling rate is higher for the early and late stages.

In our experiments, we determine the different stages of the denoising process as follows, setting $\lambda_{den} = 5$. The early stage is defined for $t \in [800, 1000]$ and we sample 10 timesteps uniformly within this interval. The middle stage is defined for $t \in [200, 800]$ and we sample 6 timesteps uniformly within this interval. The last stage is defined for $t \in [0, 200]$ and we sample 10 timesteps uniformly within this interval. In total, we sample 26 timesteps throughout the denoising process.

A.4 Ablation Study

We conduct ablation studies focused on each component on our method, and present the results for the default checkpoint of Zero-1-to-3 and for Zero123-XL. In addition to the main ablation table shown in the main paper, we present the same study on Zero-1-to-3 in Tab. 3.

Hourglass scheduling. We run the original model with 25, 50 and 100 steps sampled uniformly using DDIM, and show that the hourglass scheduling, with 26 steps sampled in total, performs better or on par. The main benefit of our Hourglass scheduling is reducing the number of steps, but it also slightly improves the overall performance. Results are presented for Zero-1-to-3 in Tab. 7 and for Zero123-XL in Tab. 4.

Table 3: **Ablation study.** We demonstrate the importance of each of Zero-to-Hero modules, applied to the base method Zero-1-to-3: Sample scheduling (Hourglass), Resampling (Resample), Attention map filtering (AMF), and Early stage Mutual Self-Attention (MSA).

Hourglass	Resample	AMF	MSA	PSNR \uparrow	SSIM \uparrow	LPIPS \downarrow	IOU \uparrow
×	×	×	×	16.72	0.851	0.181	75.6%
✓	×	×	×	16.77	0.853	0.182	75.8%
✓	✓	×	×	17.00	0.855	0.178	76.7%
✓	✓	✓	×	17.04	0.856	0.176	77.3%
✓	✓	×	✓	16.91	0.860	0.173	76.1%
✓	✓	✓	✓	17.13	0.862	0.170	77.2%

Table 4: **Ablation study: Hourglass scheduling.** We demonstrate the superiority of our Hourglass scheduling over uniform DDIM sampling with different number of denoising steps. The experiments are based on Zero123-XL.

Sampling	T	NFE	PSNR \uparrow	SSIM \uparrow	LPIPS \downarrow	IOU \uparrow
Uniform	25	25	17.16	0.856	0.174	77.8%
Uniform	50	50	17.13	0.854	0.173	77.6%
Uniform	100	100	17.13	0.854	0.173	77.6%
Hourglass	26	26	17.18	0.856	0.172	78.0%

Attention map filtering. We use the hourglass scheduling for all further experiments. We run the original model with and without resampling and attention filtering. Our experiments demonstrate that adding the attention filtering in addition to the resampling mechanism improves the performance across all metrics. Results are presented for Zero-1-to-3 in Tab. 8 and for Zero123-XL in Tab. 5.

Early-Stage mutual self-attention. Maintaining the hourglass scheduling, we first run the original model with Early-Stage mutual self-attention. Then, we compare adding resampling versus adding steps uniformly to match the effective sampling budget induced by resampling. E.g. if we perform resampling for timesteps $t \in [\tau_1, \tau_2]$ with R resampling iterations, we compare that to running the model without resampling, while multiplying the number of sampled timesteps within $[\tau_1, \tau_2]$ by a factor of R . We can see that combining resampling with mutual self-attention leads to better performance overall. Results are presented for Zero-1-to-3 in Tab. 9 and for Zero123-XL in Tab. 6.

A.5 Generation Diversity Ablation Study

While our attention filtering manages to generate more robust and consistent results, we find that it might limit the generation diversity. We explore the two main factors that can reduce the diversity: the number of filtering iterations R and the interval of timesteps $[t_{min}, t_{max}]$ where we apply filtering.

Number of filtering iterations. In Fig. 8, we show the effect of different values of R on the diversity of the results. All other hyper-parameters remain unchanged. We find that as R grows, the generation diversity reduces, while the level of realism improves

Filtering schedule. We apply filtering during timesteps $t \in [t_{min}, T]$. In Fig. 9, we show the effect of different values of t_{min} on the diversity of the results. All the hyper-parameters besides t_{min}

Table 5: **Ablation study: Attention map filtering.** We demonstrate the importance of Attention Map Filtering (AMF) over only applying Resampling (Resample). The experiments are based on Zero123-XL.

Name	T	NFE	PSNR \uparrow	SSIM \uparrow	LPIPS \downarrow	IOU \uparrow
Zero123-XL	26	26	17.18	0.856	0.172	78.0%
+ Resample	26	66	17.44	0.859	0.169	78.6%
+ Resample + AMF	26	66	17.58	0.861	0.165	79.6%

Table 6: **Ablation study: Early-stage mutual self-attention.** We demonstrate the contribution of Early-Stage Mutual Self-Attention (MSA). We also show that the combination of Early-Stage Mutual Self-Attention with Resampling (Resample) via resampling is superior to adding denoising steps to match the effective number of steps induced by resampling. The experiments are based on Zero123-XL.

Name	T	NFE	PSNR \uparrow	SSIM \uparrow	LPIPS \downarrow	IOU \uparrow
Zero123-XL	26	26	17.18	0.856	0.172	78.0%
+ MSA	26	26	17.70	0.865	0.163	79.6%
+ MSA + Adding Denoising Steps	66	66	17.67	0.864	0.165	79.4%
+ MSA + Resample	26	66	17.82	0.866	0.161	79.7%
Ours (Full)	26	66	17.90	0.867	0.159	80.3%

Table 7: **Ablation study: Hourglass scheduling.** We demonstrate the superiority of our Hourglass scheduling over uniform DDIM sampling with different number of denoising steps. The experiments are based on Zero-1-to-3.

Sampling	T	NFE	PSNR \uparrow	SSIM \uparrow	LPIPS \downarrow	IOU \uparrow
Uniform	25	25	16.65	0.851	0.185	75.5%
Uniform	50	50	16.66	0.851	0.181	75.6%
Uniform	100	100	16.72	0.851	0.184	75.6%
Hourglass	26	26	16.77	0.853	0.182	75.8%

Table 8: **Ablation study: Attention map filtering.** We demonstrate the importance of Attention Map Filtering over only applying Resampling (Resample). The experiments are based on Zero-1-to-3.

Name	T	NFE	PSNR \uparrow	SSIM \uparrow	LPIPS \downarrow	IOU \uparrow
Zero123-XL	26	26	16.77	0.853	0.182	75.8%
+ Resample	26	66	17.00	0.855	0.178	76.7%
+ Resample + AMF	26	66	17.04	0.856	0.176	77.3%

Table 9: **Ablation study: Early-stage mutual self-attention.** We demonstrate the contribution of Early-Stage Mutual Self-Attention (MSA). We also show that the combination of Early-Stage Mutual Self-Attention with Resampling (Resample) is superior to adding denoising steps to match the effective number of steps induced by resampling. The experiments are based on Zero-1-to-3.

Name	T	NFE	PSNR \uparrow	SSIM \uparrow	LPIPS \downarrow	IOU \uparrow
Zero123-XL	26	26	16.77	0.853	0.182	75.8%
+ MSA	26	26	16.93	0.859	0.175	76.5%
+ MSA + Adding Denoising Steps	66	66	17.95	0.859	0.176	76.5%
+ MSA + Resample	26	66	17.91	0.860	0.173	76.1%
Ours (Full)	26	66	17.13	0.862	0.170	77.2%

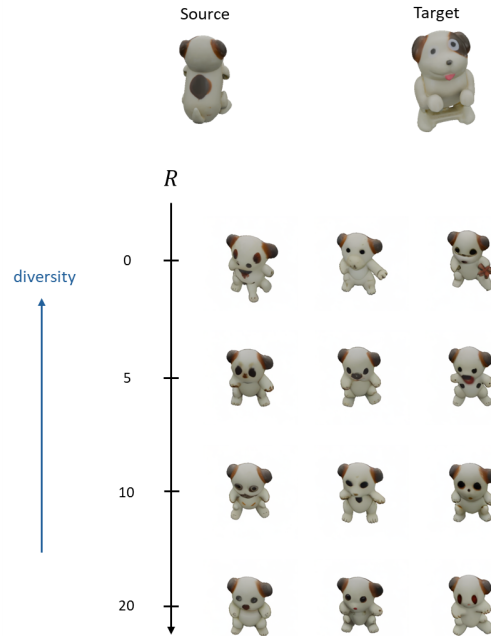


Figure 8: **Generation diversity wrt filtering iterations.** We select an extreme change in viewpoint, and show how different choices of R , the number of filtering iterations, affect the diversity of generated outputs. As filtering iterations increase, the results become less diverse and more realistic.

remain unchanged. We observe that as we apply filtering for longer periods of the denoising steps, the results are more realistic but less diverse.

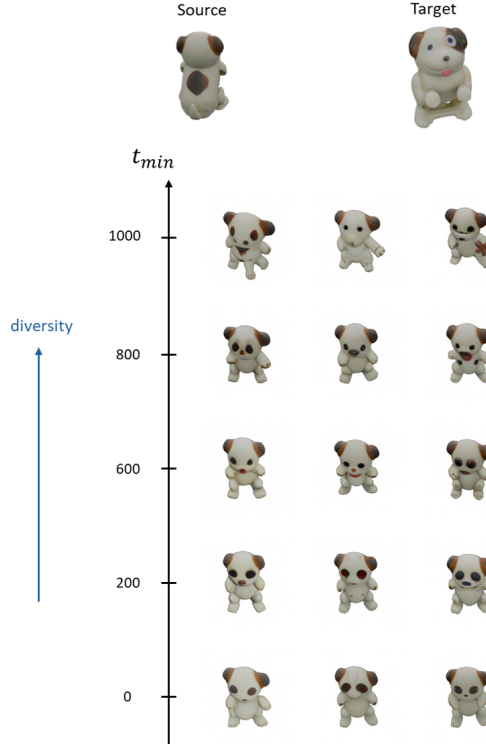


Figure 9: **Generation diversity wrt filtering schedule.** We select an extreme change in viewpoint, and show how different choices of the timesteps interval where filtering is applied, affect the diversity of results. As filtering is applied for longer periods during the denoising process, the results become less diverse and more realistic.

A.6 Data

Dataset creation. For each object, we render various views by randomly selecting camera parameters, an elevation $\theta \in [0, \pi]$, an azimuth $\phi \in [0, 2\pi]$ and a radius $r \in [1.5, 2.2]$. We manually select 8 views for each object by removing images captured from close viewpoints and filtering camera viewpoints only from the upper half of the unit sphere, to avoid significant lighting effects that swing the results regardless of the output geometry.

Dataset assets. We provide a list of the objects picked for the challenging subset of GSO. Objects listed with bold font are also used for the ablation studies.

- | | |
|---|---|
| 1. BALANCING_CACTUS | 14. adiZero_Slide_2_SC |
| 2. Chelsea_lo_fl_rdheel_nQ0LPNF1oMw | 15. Air_Hogs_Wind_Flyers_Set_Airplane_Red |
| 3. CHICKEN_RACER | 16. COAST_GUARD_BOAT |
| 4. Circo_Fish_Toothbrush_Holder_14995988 | 17. CREATIVE_BLOCKS_35_MM |
| 5. Great_Dinos_Triceratops_Toy | 18. Dino_5 |
| 6. Nintendo_Mario_Action_Figure | 19. Down_To_Earth_Ceramic_Orchid_Pot_Asst_Blue |
| 7. Ortho_Forward_Facing | 20. FIRE_ENGINE |
| 8. Sonny_School_Bus | 21. Guardians_of_the_Galaxy_Galactic_Battlers_Rocket_Raccoon_Figure |
| 9. Squirrel | 22. Hilary |
| 10. Vtech_Roll_Learn_Turtle | 23. Imaginext_Castle_Ogre |
| 11. 3D_Dollhouse_Sink | 24. My_First_Rolling_Lion |
| 12. 3D_Dollhouse_Swing | 25. My_First_Wiggle_Crocodile |
| 13. 3D_Dollhouse_TablePurple | |

26. My_Little_Pony_Princess_Celestia
27. Nickelodeon_Teenage_Mutant_Ninja_Turtles_Leonardo
28. Nickelodeon_Teenage_Mutant_Ninja_Turtles_Michelangelo
29. Nintendo_Yoshi_Action_Figure
30. Olive_Kids_Mermaids_Pack_n_Snack_Backpack
31. Ortho_Forward_Facing_3Q6J2oKJD92
32. Ortho_Forward_Facing_QCaor9ImJ2G
33. Raccoon
34. Razer_Kraken_Pro_headset_Full_size_Black
35. Remington_TStudio_Hair_Dryer
36. Rubbermaid_Large_Drainer
37. Schleich_African_Black_Rhino
38. Schleich_Hereford_Bull
39. Schleich_Lion_Action_Figure
40. Schleich_S_Bayala_Unicorn_70432
41. Smith_Hawken_Woven_BasketTray_Organizer_with_3_Compartment_95_x_9_x_13
42. Sootheze_Cold_Therapy_Elephant
43. SORTING_TRAIN
44. Toysmith_Windem_Up_Flippin_Animals_Dog
45. Transformers_Age_of_Extinction_Mega_1Step_Bumblebee_Figure
46. TriStar_Products_PPC_Power_Pressure_Cooker_XL_in_Black
47. W_Lou_z0dkC78niiZ
48. Weisshai_Great_White_Shark
49. Whey_Protein_Vanilla
50. ZX700_mzGbdP3u6JB